

Probing Strangeness Canonical Ensemble with K^- , $\phi(1020)$ and Ξ^- Production in Au+Au Collisions at $\sqrt{s_{\text{NN}}} = 3$ GeV

M. S. Abdallah,⁵ B. E. Aboona,⁵⁵ J. Adam,⁶ L. Adamczyk,² J. R. Adams,³⁹ J. K. Adkins,³⁰ G. Agakishiev,²⁸ I. Aggarwal,⁴¹ M. M. Aggarwal,⁴¹ Z. Ahammed,⁶⁰ I. Alekseev,^{3,35} D. M. Anderson,⁵⁵ A. Aparin,²⁸ E. C. Aschenauer,⁶ M. U. Ashraf,¹¹ F. G. Atetalla,²⁹ A. Attri,⁴¹ G. S. Averichev,²⁸ V. Bairathi,⁵³ W. Baker,¹⁰ J. G. Ball Cap,²⁰ K. Barish,¹⁰ A. Behera,⁵² R. Bellwied,²⁰ P. Bhagat,²⁷ A. Bhasin,²⁷ J. Bielcik,¹⁴ J. Bielcikova,³⁸ I. G. Bordyuzhin,³ J. D. Brandenburg,⁶ A. V. Brandin,³⁵ I. Bunzarov,²⁸ J. Butterworth,⁴⁵ X. Z. Cai,⁵⁰ H. Caines,⁶³ M. Calderón de la Barca Sánchez,⁸ D. Cebra,⁸ I. Chakaberia,^{31,6} P. Chaloupka,¹⁴ B. K. Chan,⁹ F-H. Chang,³⁷ Z. Chang,⁶ N. Chankova-Bunzarova,²⁸ A. Chatterjee,¹¹ S. Chattopadhyay,⁶⁰ D. Chen,¹⁰ J. Chen,⁴⁹ J. H. Chen,¹⁸ X. Chen,⁴⁸ Z. Chen,⁴⁹ J. Cheng,⁵⁷ M. Chevalier,¹⁰ S. Choudhury,¹⁸ W. Christie,⁶ X. Chu,⁶ H. J. Crawford,⁷ M. Csanád,¹⁶ M. Daugherty,¹ T. G. Dedovich,²⁸ I. M. Deppner,¹⁹ A. A. Derevschikov,⁴³ A. Dhamija,⁴¹ L. Di Carlo,⁶² L. Didenko,⁶ P. Dixit,²² X. Dong,³¹ J. L. Drachenberg,¹ E. Duckworth,²⁹ J. C. Dunlop,⁶ N. Elsey,⁶² J. Engelage,⁷ G. Eppley,⁴⁵ S. Esumi,⁵⁸ O. Evdokimov,¹² A. Ewigleben,³² O. Eyser,⁶ R. Fatemi,³⁰ F. M. Fawzi,⁵ S. Fazio,⁶ P. Federic,³⁸ J. Fedorisin,²⁸ C. J. Feng,³⁷ Y. Feng,⁴⁴ P. Filip,²⁸ E. Finch,⁵¹ Y. Fisyak,⁶ A. Francisco,⁶³ C. Fu,¹¹ L. Fulek,² C. A. Gagliardi,⁵⁵ T. Galatyuk,¹⁵ F. Geurts,⁴⁵ N. Ghimire,⁵⁴ A. Gibson,⁵⁹ K. Gopal,²³ X. Gou,⁴⁹ D. Grosnick,⁵⁹ A. Gupta,²⁷ W. Guryn,⁶ A. I. Hamad,²⁹ A. Hamed,⁵ Y. Han,⁴⁵ S. Harabasz,¹⁵ M. D. Harasty,⁸ J. W. Harris,⁶³ H. Harrison,³⁰ S. He,¹¹ W. He,¹⁸ X. H. He,²⁶ Y. He,⁴⁹ S. Heppelmann,⁸ S. Heppelmann,⁴² N. Herrmann,¹⁹ E. Hoffman,²⁰ L. Holub,¹⁴ Y. Hu,¹⁸ H. Huang,³⁷ H. Z. Huang,⁹ S. L. Huang,⁵² T. Huang,³⁷ X. Huang,⁵⁷ Y. Huang,⁵⁷ T. J. Humanic,³⁹ G. Igo,^{9,*} D. Isenhower,¹ W. W. Jacobs,²⁵ C. Jena,²³ A. Jentsch,⁶ Y. Ji,³¹ J. Jia,^{6,52} K. Jiang,⁴⁸ X. Ju,⁴⁸ E. G. Judd,⁷ S. Kabana,⁵³ M. L. Kabir,¹⁰ S. Kagamaster,³² D. Kalinkin,^{25,6} K. Kang,⁵⁷ D. Kapukchyan,¹⁰ K. Kauder,⁶ H. W. Ke,⁶ D. Keane,²⁹ A. Kechechyan,²⁸ M. Kelsey,⁶² Y. V. Khyzhniak,³⁵ D. P. Kikoła,⁶¹ C. Kim,¹⁰ B. Kimelman,⁸ D. Kincses,¹⁶ I. Kisel,¹⁷ A. Kiselev,⁶ A. G. Knospe,³² H. S. Ko,³¹ L. Kochenda,³⁵ L. K. Kosarzewski,¹⁴ L. Kramarik,¹⁴ P. Kravtsov,³⁵ L. Kumar,⁴¹ S. Kumar,²⁶ R. Kunnawalkam Elayavalli,⁶³ J. H. Kwasizur,²⁵ R. Lacey,⁵² S. Lan,¹¹ J. M. Landgraf,⁶ J. Lauret,⁶ A. Lebedev,⁶ R. Lednicky,^{28,38} J. H. Lee,⁶ Y. H. Leung,³¹ C. Li,⁴⁹ C. Li,⁴⁸ W. Li,⁴⁵ X. Li,⁴⁸ Y. Li,⁵⁷ X. Liang,¹⁰ Y. Liang,²⁹ R. Licenik,³⁸ T. Lin,⁴⁹ Y. Lin,¹¹ M. A. Lisa,³⁹ F. Liu,¹¹ H. Liu,²⁵ H. Liu,¹¹ P. Liu,⁵² T. Liu,⁶³ X. Liu,³⁹ Y. Liu,⁵⁵ Z. Liu,⁴⁸ T. Ljubicic,⁶ W. J. Llope,⁶² R. S. Longacre,⁶ E. Loyd,¹⁰ N. S. Lukow,⁵⁴ X. F. Luo,¹¹ L. Ma,¹⁸ R. Ma,⁶ Y. G. Ma,¹⁸ N. Magdy,¹² D. Mallick,³⁶ S. Margetis,²⁹ C. Markert,⁵⁶ H. S. Matis,³¹ J. A. Mazer,⁴⁶ N. G. Minaev,⁴³ S. Mioduszewski,⁵⁵ B. Mohanty,³⁶ M. M. Mondal,⁵² I. Mooney,⁶² D. A. Morozov,⁴³ A. Mukherjee,¹⁶ M. Nagy,¹⁶ J. D. Nam,⁵⁴ Md. Nasim,²² K. Nayak,¹¹ D. Neff,⁹ J. M. Nelson,⁷ D. B. Nemes,⁶³ M. Nie,⁴⁹ G. Nigmatkulov,³⁵ T. Niida,⁵⁸ R. Nishitani,⁵⁸ L. V. Nogach,⁴³ T. Nonaka,⁵⁸ A. S. Nunes,⁶ G. Odyniec,³¹ A. Ogawa,⁶ S. Oh,³¹ V. A. Okorokov,³⁵ B. S. Page,⁶ R. Pak,⁶ J. Pan,⁵⁵ A. Pandav,³⁶ A. K. Pandey,⁵⁸ Y. Panebratsev,²⁸ P. Parfenov,³⁵ B. Pawlik,⁴⁰ D. Pawlowska,⁶¹ H. Pei,¹¹ C. Perkins,⁷ L. Pinsky,²⁰ R. L. Pintér,¹⁶ J. Pluta,⁶¹ B. R. Pokhrel,⁵⁴ G. Pomatkin,³⁸ J. Porter,³¹ M. Posik,⁵⁴ V. Prozorova,¹⁴ N. K. Pruthi,⁴¹ M. Przybycien,² J. Putschke,⁶² H. Qiu,²⁶ A. Quintero,⁵⁴ C. Racz,¹⁰ S. K. Radhakrishnan,²⁹ N. Raha,⁶² R. L. Ray,⁵⁶ R. Reed,³² H. G. Ritter,³¹ M. Robotkova,³⁸ O. V. Rogachevskiy,²⁸ J. L. Romero,⁸ D. Roy,⁴⁶ L. Ruan,⁶ J. Rusnak,³⁸ N. R. Sahoo,⁴⁹ H. Sako,⁵⁸ S. Salur,⁴⁶ J. Sandweiss,^{63,*} S. Sato,⁵⁸ W. B. Schmidke,⁶ N. Schmitz,³³ B. R. Schweid,⁵² F. Seck,¹⁵ J. Seger,¹³ M. Sergeeva,⁹ R. Seto,¹⁰ P. Seyboth,³³ N. Shah,²⁴ E. Shahaliev,²⁸ P. V. Shanmuganathan,⁶ M. Shao,⁴⁸ T. Shao,¹⁸ A. I. Sheikh,²⁹ D. Shen,⁵⁰ S. S. Shi,¹¹ Y. Shi,⁴⁹ Q. Y. Shou,¹⁸ E. P. Sichtermann,³¹ R. Sikora,² M. Simko,³⁸ J. Singh,⁴¹ S. Singha,²⁶ M. J. Skoby,⁴⁴ N. Smirnov,⁶³ Y. Söhnngen,¹⁹ W. Solyst,²⁵ P. Sorensen,⁶ H. M. Spinka,^{4,*} B. Srivastava,⁴⁴ T. D. S. Stanislaus,⁵⁹ M. Stefaniak,⁶¹ D. J. Stewart,⁶³ M. Strikhanov,³⁵ B. Stringfellow,⁴⁴ A. A. P. Suaide,⁴⁷ M. Sumera,³⁸ B. Summa,⁴² X. M. Sun,¹¹ X. Sun,¹² Y. Sun,⁴⁸ Y. Sun,²¹ B. Surrow,⁵⁴ D. N. Svirida,³ Z. W. Sweger,⁸ P. Szymanski,⁶¹ A. H. Tang,⁶ Z. Tang,⁴⁸ A. Taranenko,³⁵ T. Tarnowsky,³⁴ J. H. Thomas,³¹ A. R. Timmins,²⁰ D. Tlusty,¹³ T. Todoroki,⁵⁸ M. Tokarev,²⁸ C. A. Tomkiel,³² S. Trentalange,⁹ R. E. Tribble,⁵⁵ P. Tribedy,⁶ S. K. Tripathy,¹⁶ T. Truhlar,¹⁴ B. A. Trzeciak,¹⁴ O. D. Tsai,⁹ Z. Tu,⁶ T. Ullrich,⁶ D. G. Underwood,^{4,59} I. Upsal,⁴⁵ G. Van Buren,⁶ J. Vanek,³⁸ A. N. Vasiliev,⁴³ I. Vassiliev,¹⁷ V. Verkest,⁶² F. Videbæk,⁶ S. Vokal,²⁸ S. A. Voloshin,⁶² F. Wang,⁴⁴ G. Wang,⁹ J. S. Wang,²¹ P. Wang,⁴⁸ Y. Wang,¹¹ Y. Wang,⁵⁷ Z. Wang,⁴⁹ J. C. Webb,⁶ P. C. Weidenkaff,¹⁹ L. Wen,⁹ G. D. Westfall,³⁴ H. Wieman,³¹ S. W. Wissink,²⁵ J. Wu,²⁶ Y. Wu,¹⁰ B. Xi,⁵⁰ Z. G. Xiao,⁵⁷ G. Xie,³¹ W. Xie,⁴⁴ H. Xu,²¹ N. Xu,³¹ Q. H. Xu,⁴⁹ Y. Xu,⁴⁹ Z. Xu,⁶ Z. Xu,⁹ C. Yang,⁴⁹ Q. Yang,⁴⁹ S. Yang,⁴⁵ Y. Yang,³⁷ Z. Ye,⁴⁵ Z. Ye,¹² L. Yi,⁴⁹ K. Yip,⁶ Y. Yu,⁴⁹ H. Zbroszczyk,⁶¹ W. Zha,⁴⁸ C. Zhang,⁵² D. Zhang,¹¹ J. Zhang,⁴⁹ S. Zhang,¹² S. Zhang,¹⁸ X. P. Zhang,⁵⁷ Y. Zhang,²⁶ Y. Zhang,⁴⁸ Y. Zhang,¹¹ Z. J. Zhang,³⁷ Z. Zhang,⁶ Z. Zhang,¹² J. Zhao,⁴⁴ C. Zhou,¹⁸ X. Zhu,⁵⁷ M. Zurek,⁴ and M. Zyzak¹⁷

(STAR Collaboration)

- ¹Abilene Christian University, Abilene, Texas 79699
- ²AGH University of Science and Technology, FPACS, Cracow 30-059, Poland
- ³Alikhanov Institute for Theoretical and Experimental Physics NRC "Kurchatov Institute", Moscow 117218, Russia
- ⁴Argonne National Laboratory, Argonne, Illinois 60439
- ⁵American University of Cairo, New Cairo 11835, New Cairo, Egypt
- ⁶Brookhaven National Laboratory, Upton, New York 11973
- ⁷University of California, Berkeley, California 94720
- ⁸University of California, Davis, California 95616
- ⁹University of California, Los Angeles, California 90095
- ¹⁰University of California, Riverside, California 92521
- ¹¹Central China Normal University, Wuhan, Hubei 430079
- ¹²University of Illinois at Chicago, Chicago, Illinois 60607
- ¹³Creighton University, Omaha, Nebraska 68178
- ¹⁴Czech Technical University in Prague, FNSPE, Prague 115 19, Czech Republic
- ¹⁵Technische Universität Darmstadt, Darmstadt 64289, Germany
- ¹⁶ELTE Eötvös Loránd University, Budapest, Hungary H-1117
- ¹⁷Frankfurt Institute for Advanced Studies FIAS, Frankfurt 60438, Germany
- ¹⁸Fudan University, Shanghai, 200433
- ¹⁹University of Heidelberg, Heidelberg 69120, Germany
- ²⁰University of Houston, Houston, Texas 77204
- ²¹Huzhou University, Huzhou, Zhejiang 313000
- ²²Indian Institute of Science Education and Research (IISER), Berhampur 760010, India
- ²³Indian Institute of Science Education and Research (IISER) Tirupati, Tirupati 517507, India
- ²⁴Indian Institute Technology, Patna, Bihar 801106, India
- ²⁵Indiana University, Bloomington, Indiana 47408
- ²⁶Institute of Modern Physics, Chinese Academy of Sciences, Lanzhou, Gansu 730000
- ²⁷University of Jammu, Jammu 180001, India
- ²⁸Joint Institute for Nuclear Research, Dubna 141 980, Russia
- ²⁹Kent State University, Kent, Ohio 44242
- ³⁰University of Kentucky, Lexington, Kentucky 40506-0055
- ³¹Lawrence Berkeley National Laboratory, Berkeley, California 94720
- ³²Lehigh University, Bethlehem, Pennsylvania 18015
- ³³Max-Planck-Institut für Physik, Munich 80805, Germany
- ³⁴Michigan State University, East Lansing, Michigan 48824
- ³⁵National Research Nuclear University MPhI, Moscow 115409, Russia
- ³⁶National Institute of Science Education and Research, HBNI, Jatni 752050, India
- ³⁷National Cheng Kung University, Tainan 70101
- ³⁸Nuclear Physics Institute of the CAS, Rez 250 68, Czech Republic
- ³⁹Ohio State University, Columbus, Ohio 43210
- ⁴⁰Institute of Nuclear Physics PAN, Cracow 31-342, Poland
- ⁴¹Panjab University, Chandigarh 160014, India
- ⁴²Pennsylvania State University, University Park, Pennsylvania 16802
- ⁴³NRC "Kurchatov Institute", Institute of High Energy Physics, Protvino 142281, Russia
- ⁴⁴Purdue University, West Lafayette, Indiana 47907
- ⁴⁵Rice University, Houston, Texas 77251
- ⁴⁶Rutgers University, Piscataway, New Jersey 08854
- ⁴⁷Universidade de São Paulo, São Paulo, Brazil 05314-970
- ⁴⁸University of Science and Technology of China, Hefei, Anhui 230026
- ⁴⁹Shandong University, Qingdao, Shandong 266237
- ⁵⁰Shanghai Institute of Applied Physics, Chinese Academy of Sciences, Shanghai 201800
- ⁵¹Southern Connecticut State University, New Haven, Connecticut 06515
- ⁵²State University of New York, Stony Brook, New York 11794
- ⁵³Instituto de Alta Investigación, Universidad de Tarapacá, Arica 1000000, Chile
- ⁵⁴Temple University, Philadelphia, Pennsylvania 19122
- ⁵⁵Texas A&M University, College Station, Texas 77843
- ⁵⁶University of Texas, Austin, Texas 78712
- ⁵⁷Tsinghua University, Beijing 100084
- ⁵⁸University of Tsukuba, Tsukuba, Ibaraki 305-8571, Japan
- ⁵⁹Valparaiso University, Valparaiso, Indiana 46383
- ⁶⁰Variable Energy Cyclotron Centre, Kolkata 700064, India
- ⁶¹Warsaw University of Technology, Warsaw 00-661, Poland
- ⁶²Wayne State University, Detroit, Michigan 48201

⁶³Yale University, New Haven, Connecticut 06520

(Dated: March 22, 2022)

We report on the first multi-differential measurement of ϕ meson and Ξ^- hyperon production as well as the ϕ/K^- and ϕ/Ξ^- ratio in Au+Au collisions at $\sqrt{s_{\text{NN}}} = 3$ GeV with the STAR experiment under its fixed target configuration at RHIC. ϕ mesons and Ξ^- hyperons are measured through their hadronic decay channels, $\phi \rightarrow K^+K^-$ and $\Xi^- \rightarrow \Lambda\pi^-$. The transverse kinetic energy spectra of K^- , ϕ and Ξ^- are presented in different centrality and rapidity intervals. The total production yields and the ratios within a 4π coverage are calculated and compared to thermal model predictions. A calculation within the grand canonical ensemble framework shows a clear discrepancy from our measurement. Our data favor the canonical ensemble approach employing local strangeness conservation with a small strangeness correlation length ($r_c \leq 4.2$ fm) in 0–10% central Au+Au collisions at $\sqrt{s_{\text{NN}}} = 3$ GeV.

Relativistic heavy ion physics is aiming at the detailed investigation of phase structures of strongly interacting matter, governed by quantum chromodynamics (QCD), under extreme conditions of high temperature and density [1–3]. Particle production has been studied to investigate the properties of the produced QCD matter in heavy-ion collisions. The strange quark mass is comparable to the QCD renormalization scale ($\Lambda_{\text{QCD}} \sim 200$ MeV) [4, 5], therefore strange quark dynamics plays an important role in understanding the QCD Equation-of-State of hot and dense nuclear matter particularly in the high density region [6–11].

Statistical thermal models have often been used to characterize the thermal properties of the produced media [12–16]. In these models, grand canonical ensemble (GCE) and canonical ensemble (CE) statistical descriptions can be applied to conserve electric charge, baryon number, and strangeness number in order to compute the final state particle yields. Both GCE and CE models are able to describe various particle yields including strange particles produced in heavy-ion collisions at RHIC and the LHC at center-of-mass energy ($\sqrt{s_{\text{NN}}}$) greater than 7.7 GeV. It has been argued that at lower energies, strangeness number needs to be conserved locally on an event-by-event basis described by the CE, which leads to a reduction in the yields of hadrons with non-zero strangeness number (“Canonical Suppression”) [17].

The $\phi(1020)$ meson is the lightest bound state of strange quarks into a pair ($s\bar{s}$) with zero net strangeness number ($S=0$). In the GCE model, the ϕ/K^- ratio is expected to fall off as the collision energy decreases towards the threshold. In the CE model, ϕ meson production, unlike other strange hadrons (K^- , Ξ^- , etc.), is not affected by the strangeness canonical suppression. Therefore, the ϕ/K^- ratio is expected to increase with decreasing collision energy in models using the CE treatment for strangeness. The canonical suppression power for Ξ^- is even larger than for K^- . The ϕ/K^- and ϕ/Ξ^- ratios offer a unique test to scrutinize thermodynamic properties of strange quarks in the hot and dense QCD environment.

In heavy-ion collisions, the near/sub-threshold production of multi-strange hadrons can be achieved from the multiple collisions of nucleons, produced particles, and short-lived resonances [18]. The particle production in heavy-ion collisions below its free nucleon-nucleon (NN) threshold ($\sqrt{s_{\text{NN}}} \sim 2.89$ GeV for ϕ and ~ 3.25 GeV for Ξ^-) is expected to be sensitive to the stiffness of the nuclear equation of state at high density, as it is for single-strange hadrons [9, 19]. The near/sub-threshold production further provides the possibility to observe exotic states of QCD matter [20] and signatures of “soft deconfinement” [21].

Measurements from the experiments at the AGS, SPS, RHIC and LHC show that the ϕ/K^- ratio in heavy-ion collisions stays remarkably flat (~ 0.15) at collision energies $\sqrt{s_{\text{NN}}} > 5$ GeV [22–24]. Recent measurements of the ϕ/K^- ratio in heavy-ion collisions at collision energies below the ϕ free NN-threshold from HADES and FOPI show a hint of relative enhancement compared to those from high energies at RHIC and the LHC [25–28], indicative of the applicability of the CE description for strangeness production at these energies. The RHIC Beam Energy Scan phase-II program, including both collider and fixed target setups with the STAR experiment, covers a center-of-mass energy range of 3.0–19.6 GeV. This offers a great opportunity to conduct precise measurements of the energy dependence of the ϕ/K^- and ϕ/Ξ^- ratios at low collision energies, which are crucial in understanding the strangeness dynamics as well as the medium properties in high baryon density regions in QCD.

The dataset used in this analysis consists of Au+Au collisions at $\sqrt{s_{\text{NN}}} = 3$ GeV collected by the STAR experiment operated under the fixed target (FXT) setup [29] in the 2018 RHIC run. A single beam was provided by RHIC with total energy equal to 3.85 GeV/nucleon and incident on a gold target of thickness 0.25 mm, corresponding to a 1% interaction probability. The target is installed inside the vacuum pipe, 2 cm below the center of the beam axis, and located 200 cm to the west of the center of the STAR detector. The main detectors used are the Time Projection Chamber (TPC) [30], the Time of Flight (TOF) detector [31], and the Beam-Beam Counter (BBC) [32]. The trigger is provided by the signal in the east BBC detector and at least five hits in the TOF detec-

* Deceased

tor. Tracking and particle identification (PID) are done using the TPC and TOF. Events are selected with the offline reconstructed collision vertex within 1.5 cm of the target center along the beam direction. Approximately 2.6×10^8 minimum bias (MB) triggered events passed the selection criteria and are used in this analysis.

The centrality class is selected using measured charged particle multiplicity within the TPC acceptance. A Monte Carlo Glauber model, used in conjunction with a negative binomial distribution to model particle production in hadronic collisions, is optimized in order to best match the data and determine the centrality class. Due to the trigger inefficiency in the low multiplicity region (corresponding to the most peripheral collisions), and finite contribution to our signals of interest, we only report the results from the 0–60% (0–40%) centrality class in this paper.

The ϕ mesons are reconstructed via the hadronic decay channel $\phi \rightarrow K^+K^-$ with a branching ratio (BR) of 49.2%, while the Ξ^- hyperons via the $\Xi^- \rightarrow \Lambda\pi^- \rightarrow p\pi^-\pi^-$ channel with a BR of 63.8% [33]. Ξ^- reconstruction is performed using the KF Particle Finder package based on the Kalman Filter method [34, 35]. The charged tracks are reconstructed with the TPC in a 0.5 T uniform magnetic field. The TPC tracks are required to consist of at least 20 TPC hits (out of a maximum of 45, and ratio ≥ 0.52) to ensure good tracking and avoid track splitting (15 TPC hits required for Ξ^- to increase the sample of signal candidates). The charged tracks are identified via a combination of the ionization energy loss measurement with the TPC and the time-of-flight measurement with the TOF. A minimum p_T cut of 0.2 GeV/c is required in the analysis. Due to the charge asymmetry for the particle yields at $\sqrt{s_{NN}} = 3$ GeV, a smaller yield for K^- compared to K^+ means relatively higher contamination. Thus a strict PID criterion requiring both TPC and TOF is implemented for K^- [36, 37]. Both the TPC and TOF detectors have full azimuthal coverage within a pseudorapidity range of $0 < \eta < 1.88$ for the TPC and $0 < \eta < 1.5$ for the TOF in FXT mode [30, 31].

Figure 1 (a) shows the invariant mass distribution of K^+K^- pairs in the transverse momentum (p_T) region of 0.4–1.6 GeV/c for 0–60% central collisions. The combinatorial background is estimated with the mixed-event (ME) technique in which K^+ and K^- from different events of similar characteristics (centrality, event plane angle) are paired. The mixed-event spectra are normalized to the same-event (SE) distributions in the mass range of 1.04–1.08 GeV/c². After the subtraction of the combinatorial background, the remainder distribution is shown as red solid circles. The K^+K^- invariant mass remainder distribution is fitted with a Breit-Wigner function for the signal plus a linear function which represents the remaining correlated background ($< 1\%$) from a partial reconstruction of strange hadrons. The ϕ meson raw yields are extracted from the Breit-Wigner function fit within the corresponding 3σ mass window. The extracted ϕ signal shape is consistent with its intrinsic

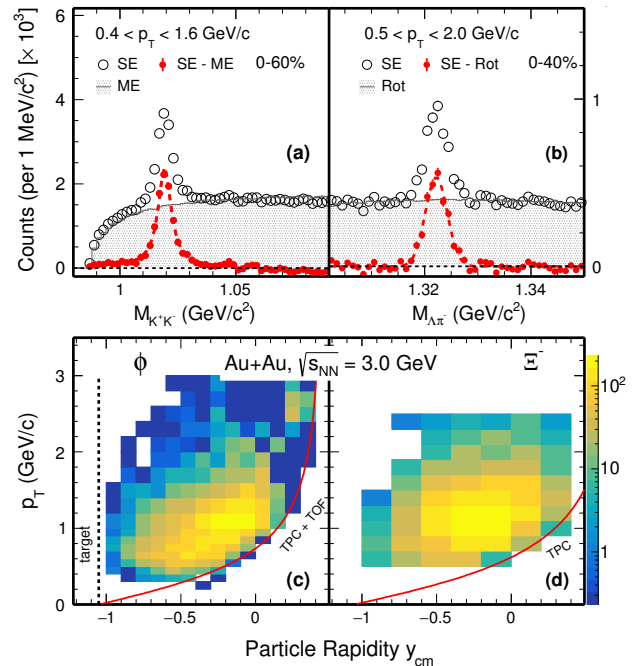


FIG. 1. Invariant mass distributions of K^+K^- ($\Lambda\pi^-$) in the p_T region of 0.4–1.6 (0.5–2.0) GeV/c in 0–60% (0–40%) central Au+Au collisions at $\sqrt{s_{NN}} = 3$ GeV. Black open circles represent the same-event unlike-sign distribution. The grey shaded histogram represents the normalized mixed-event (rotating daughters for Ξ^-) unlike-sign distribution that is used to estimate the combinatorial background. The red solid circles depict the ϕ meson (a) and Ξ^- (b) signals obtained by subtracting the combinatorial background from the same-event distribution. Reconstructed ϕ meson (c) and Ξ^- hyperon (d) acceptance plot, p_T vs. rapidity in the center-of-mass frame (y_{cm}) in Au+Au collisions at $\sqrt{s_{NN}} = 3$ GeV. The dotted line indicates the target rapidity location. The red curve represents the TPC and TOF acceptance edge.

sic properties convoluted with the detector smearing effect due to finite momentum resolution ($< 3\%$ for single track). Figure 1 (b) shows the invariant mass distribution of $\Lambda(\pi\pi^-)\pi^-$ in the p_T region of 0.5–2.0 GeV/c for 0–40% central collisions. The combinatorial background is estimated with the rotating daughter (Rot) method, in which a daughter track of Ξ^- is rotated by a random angle between 150 to 210 degrees in the transverse plane. The rotated spectra are normalized to the same-event distributions in the mass ranges of 1.30–1.31 and 1.34–1.35 GeV/c². After the combinatorial background is subtracted, the $\Lambda\pi^-$ invariant mass distributions are fitted with a Gaussian for the signal plus a linear function for the remaining correlated background. The Ξ^- raw yields are obtained via histogram bin counting from the invariant mass distributions with all background subtracted within mass windows of 3σ . The reconstructed ϕ meson and Ξ^- acceptances (p_T vs. y_{cm}) in the collision center-of-mass frame are shown in Fig. 1 (c) and (d), respectively. The target is located around $y_{cm} = -$

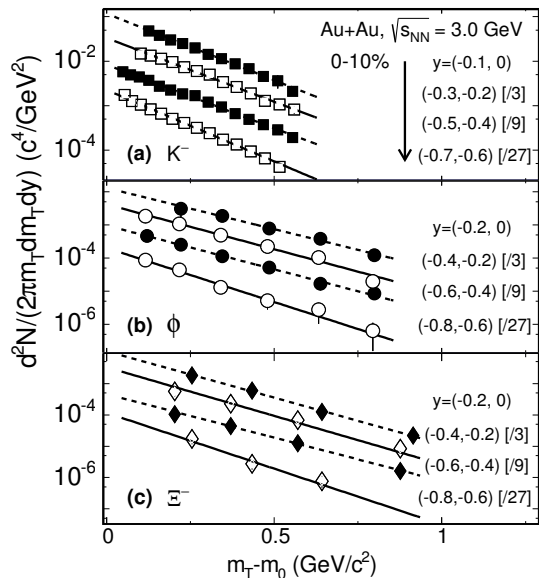


FIG. 2. K^- (a), ϕ meson (b) and Ξ^- (c) invariant yields as a function of $m_T - m_0$ for various rapidity regions in 0–10% central Au+Au collisions at $\sqrt{s_{NN}} = 3$ GeV. Statistical and systematic uncertainties are added quadratically here for plotting. Solid and dashed black lines depict m_T exponential function fits to the measured data points with scaling factors in each rapidity windows.

1.05, using the convention where the beam travels in the positive direction. The red curve represents the TPC and TOF acceptance edge. The reconstructed ϕ mesons and Ξ hyperons in this analysis cover the range from the target to mid-rapidity.

The reconstructed K^- , ϕ meson, and Ξ^- raw yields are calculated in each centrality and p_T bin within each rapidity slice. The raw yields are corrected for the TPC acceptance and tracking efficiency, the particle identification efficiency, and the TOF matching and PID efficiency. The final average reconstruction (including acceptance etc.) efficiency is about 0.30 for the K^- , about 0.04 for the ϕ meson and about 0.02 for the Ξ^- .

The systematic uncertainty of the raw yield extraction is estimated by changing the histogram fitting method to bin counting method or by changing the fitting ranges. The maximum difference between these scenarios is then converted to a standard deviation and added to the systematic uncertainties. The contribution varies by p_T , rapidity, and centrality and the overall contribution is less than 5% for the invariant yield. The systematic uncertainty in the TPC acceptance and efficiency correction ϵ_{TPC} is estimated by varying the cuts on track selection criteria and topological variables (for Ξ^- only). The contribution to the total yield is about 4–5% for K^- , 13–16% for ϕ and 6–10% for Ξ^- . This leads to a 10–13% (12–18%) uncertainty in the measured ϕ/K^- (ϕ/Ξ^-) ratio. The uncertainty of the PID efficiency correction is estimated in a similar way by varying the PID selection

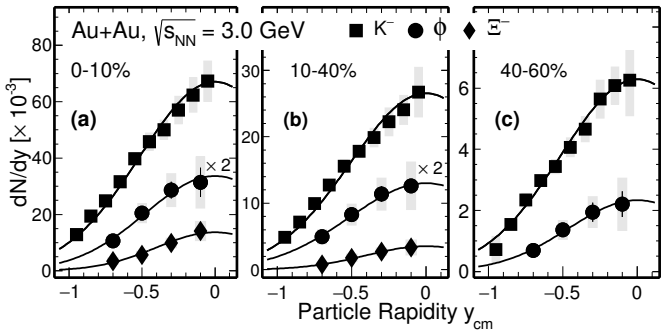


FIG. 3. Rapidity density distributions of K^- (squares), ϕ meson (circles) and Ξ^- (diamonds) p_T -integrated yields dN/dy in 0–10% (a), 10–40% (b) and 40–60% (c) Au+Au collisions at $\sqrt{s_{NN}} = 3$ GeV. Solid lines depict Gaussian function fits to the data points.

cuts and the contribution is less than 3% to the total yield. For the p_T integrated yield, one important source of systematic uncertainty comes from the extrapolation to the full p_T range due to the limited acceptance. This is estimated by choosing several fitting functions [38]. The maximum difference between these scenarios and the default one (m_T -exponential) is quoted as the systematic uncertainty from this source. This contribution is 5–7% for K^- , 14–17% for ϕ and 13–15% for Ξ^- .

Figure 2 shows the acceptance \times efficiency corrected K^- , ϕ meson and Ξ^- invariant yields as a function of transverse mass kinetic energy ($m_T - m_0$) for various rapidity ranges in 0–10% central Au+Au collisions at $\sqrt{s_{NN}} = 3$ GeV. Dashed and solid lines depict fits to the spectra with the m_T -exponential function in order to extrapolate the unmeasured p_T ranges. The p_T integrated rapidity distributions dN/dy are displayed in Fig. 3 for Au+Au collisions at $\sqrt{s_{NN}} = 3$ GeV for three different centralities. Solid curves depict Gaussian function fits to the data points with the centroid parameter fixed to zero. They are used to extrapolate to the unmeasured rapidity region in order to calculate the total multiplicities per triggered event for each particle.

The ϕ/K^- and ϕ/Ξ^- ratios is presented in Fig. 4 as a function of collision energy $\sqrt{s_{NN}}$, including the mid-rapidity data from the AGS, SPS and RHIC BES at higher energies and 4π acceptance data (weak y -dependence) from SIS at lower energies. The black solid circles show our measurements in 0–10% centrality bins in Au+Au collisions at $\sqrt{s_{NN}} = 3$ GeV. The measured ϕ , K^- and Ξ^- yields in 4π and the ϕ/K^- , ϕ/Ξ^- ratios in different centrality bins are listed in Tab. I. The ϕ/K^- and ϕ/Ξ^- ratios measured at 3 GeV are slightly higher than the values at high energies for $\sqrt{s_{NN}} \geq 5$ GeV [22–24, 39, 45–48] despite the collision energy being very close to the ϕ threshold and below the Ξ^- threshold in NN collisions. Though there is no clear difference in the ϕ/K^- ratio between the 0–10% and 10–40% central bins, the result in the most peripheral 40–60% central bin shows a hint of a

TABLE I. ϕ , K^- , Ξ^- integrated yields and ϕ/K^- and ϕ/Ξ^- ratios for given centrality classes in Au+Au collisions at $\sqrt{s_{NN}} = 3$ GeV. The first error given corresponds to the statistical one, the second to the systematic error.

Centrality	ϕ (10^{-3})	K^- (10^{-2})	ϕ/K^-	Ξ^- (10^{-3})	ϕ/Ξ^-
0–10%	$20.1 \pm 1.4 \pm 3.8$	$8.70 \pm 0.02 \pm 0.53$	$0.231 \pm 0.016 \pm 0.042$	$13.9 \pm 0.8 \pm 2.4$	$1.45 \pm 0.13 \pm 0.34$
10–40%	$8.5 \pm 0.4 \pm 1.7$	$3.39 \pm 0.01 \pm 0.20$	$0.249 \pm 0.011 \pm 0.046$	$3.61 \pm 0.32 \pm 0.59$	$2.34 \pm 0.23 \pm 0.65$
40–60%	$2.6 \pm 0.2 \pm 0.5$	$0.79 \pm 0.01 \pm 0.06$	$0.327 \pm 0.029 \pm 0.069$	—	—

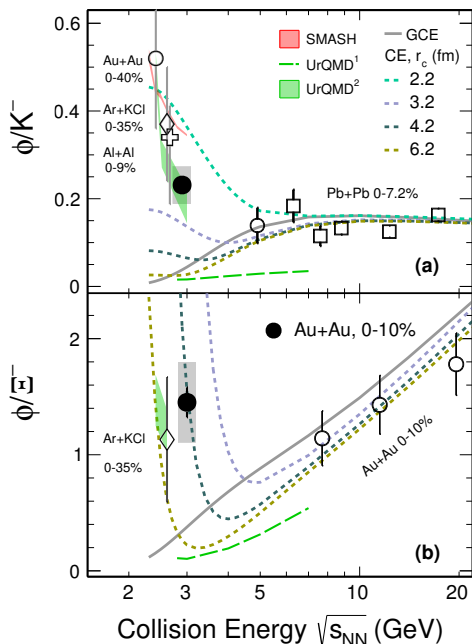


FIG. 4. ϕ/K^- (a) and ϕ/Ξ^- (b) ratio as a function of collision energy, $\sqrt{s_{NN}}$. The solid black circles show the measurements presented here in 0–10% centrality bin, while empty markers in black are used for data from various other energies and/or collision systems [22–28, 39]. The vertical grey bands on the data points represent the systematic uncertainties. The grey solid line represents a THERMUS calculation based on the Grand Canonical Ensemble (GCE) while the dotted lines depict calculations based on the Canonical Ensemble (CE) with different values of the strangeness correlation radius (r_c) [12, 40]. The green dashed line, green shaded band and the solid red line show transport model calculations from the public versions UrQMD¹ [41, 42], modified UrQMD² [43] and SMASH [44], respectively.

larger value, as shown in Tab. I. For comparison, a previous measurement in $p+p$ collisions at 2.7 GeV shows that $\phi/K^- = 1.04 \pm 0.23$ [49]. Similarly, the ϕ/Ξ^- ratio in mid-central collisions seems to be larger than that in central collisions.

Various curves in Fig. 4 represent the predictions of ϕ/K^- and ϕ/Ξ^- ratios from several model calculations in central A+A collisions. Statistical model calculations, based on the Grand Canonical Ensemble and Canonical Ensemble for strangeness with several different choices of strangeness correlation length (r_c), were calculated us-

ing the THERMUS package [40] with energy dependent freeze-out parameters (T_{ch} , μ_B) taken from [12]. These parameters were extracted through a thermal model fit to the particle yield at mid-rapidity. The strangeness number is conserved on average in the GCE, where the model does not contain a strangeness suppression factor that accounts for non-equilibrium in the strangeness sector. It is clear that the model fails to describe the data at low energies, including our new measurements at $\sqrt{s_{NN}} = 3$ GeV, which indicates the thermal particle phase-space at low energies is far from the GCE limit and the local treatment of strangeness conservation is crucial [50]. In the canonical approach, the correlation length, r_c , defines a region of the particle production phase space inside which the production of the open strangeness is canonically conserved. Both the ϕ/K^- and ϕ/Ξ^- data from our measurement favor the CE thermodynamics for strangeness with a small strangeness correlation length ($r_c \leq 4.2$ fm). It is worthwhile to point out that the CE calculations with the same r_c parameter cannot describe our ϕ/K^- and ϕ/Ξ^- data simultaneously (as also observed in lighter systems and at lower collision energy [27]). The production yields of ϕ and Ξ^- in near/sub-threshold regions based on the thermal model calculations are sensitive to the freeze-out parameters. A global thermal model fit with all the particle yields at 3 GeV will help to precisely determine these thermal parameters in the future.

Hadronic transport models are widely used in the high baryon density region to study the properties of the produced dense matter [41–44, 51, 52]. In the modified version of the Ultra-relativistic Quantum Molecular Dynamics (UrQMD) model [43], new decay channels from high mass baryon resonances to ϕ and Ξ^- are deployed. The relevant decay branching fraction was determined by fitting the experimental data from $p+p$ collisions [49]. From the comparison shown in Fig. 4, the modified UrQMD² calculation for central ($b < 5$ fm) Au+Au collisions agrees with the data points at low $\sqrt{s_{NN}}$, including our new measurement for ϕ/K^- . However calculations from the public UrQMD¹ model underestimate our measurements for both ϕ/K^- and ϕ/Ξ^- . Another hadronic transport approach called Simulating Many Accelerated Strongly-interacting Hadrons (SMASH) attempts to incorporate the newest available experimental data from both elementary hadronic cross sections and dilepton invariant mass spectra to constrain the resonance branching ratios [44]. The ϕ/K^- ratio is reasonably reproduced using SMASH in the smaller system and $\sqrt{s_{NN}}$ below

3 GeV, despite the overestimation of each individual (ϕ , K^-) transverse mass spectrum measured, e.g. in Au+Au 0-40% system by HADES [28, 44]. The predicted ϕ/K^- ratio from the same model is about 2.5σ higher than central Au+Au 0-10% collisions at 3 GeV. This indicates some important in-medium mechanism for strangeness production and propagation may be missing for the large system in SMASH.

In summary, we report the first multi-differential measurement of K^- , $\phi(1020)$ and Ξ^- production yields and the ϕ/K^- , ϕ/Ξ^- ratios in Au+Au collisions at $\sqrt{s_{NN}} = 3$ GeV with the STAR experiment at RHIC. The measured ϕ/K^- ratio is about 5σ larger than zero in 0-10% and 10-40% central collisions. The statistical model prediction based on the Grand Canonical Ensemble underestimates the measured ϕ/K^- ratio. Both the results of ϕ/K^- and ϕ/Ξ^- ratios favor the model with the Canonical Ensemble treatment for strangeness and a small strangeness correlation length parameter, r_c , in 0-10% central Au+Au collisions. The transport models including the resonance decays can reasonably describe both our measured ϕ/K^- ratio result at this energy and the trend of ϕ/Ξ^- at lower energies. Our results suggest a significant change in the strangeness production at $\sqrt{s_{NN}} = 3$ GeV compared to higher collision energies, providing new insights into the Equation-of-State of QCD matter in the high baryon density region close to the strangeness production threshold [6]. Furthermore, the sub-threshold Ξ^- measurement could serve as a probe of

a new state of QCD matter and the energy dissipation during the collision in the future [10, 53].

We would like to thank K. Redlich and J. Steinheimer for fruitful discussions. We thank the RHIC Operations Group and RCF at BNL, the NERSC Center at LBNL, and the Open Science Grid consortium for providing resources and support. This work was supported in part by the Office of Nuclear Physics within the U.S. DOE Office of Science, the U.S. National Science Foundation, the Ministry of Education and Science of the Russian Federation, National Natural Science Foundation of China, Chinese Academy of Science, the Ministry of Science and Technology of China and the Chinese Ministry of Education, the Higher Education Sprout Project by Ministry of Education at NCKU, the National Research Foundation of Korea, Czech Science Foundation and Ministry of Education, Youth and Sports of the Czech Republic, Hungarian National Research, Development and Innovation Office, New National Excellency Programme of the Hungarian Ministry of Human Capacities, Department of Atomic Energy and Department of Science and Technology of the Government of India, the National Science Centre of Poland, the Ministry of Science, Education and Sports of the Republic of Croatia, RosAtom of Russia and German Bundesministerium für Bildung, Wissenschaft, Forschung und Technologie (BMBF), Helmholtz Association, Ministry of Education, Culture, Sports, Science, and Technology (MEXT) and Japan Society for the Promotion of Science (JSPS).

-
- [1] Y. Akiba *et al.*, (2015), arXiv:1502.02730 [nucl-ex].
- [2] W. Busza, K. Rajagopal, and W. van der Schee, *Ann. Rev. Nucl. Part. Sci.* **68**, 339 (2018).
- [3] J. Adams *et al.* (STAR), *Nucl. Phys. A* **757**, 102 (2005).
- [4] J. Rafelski and B. Muller, *Phys. Rev. Lett.* **48**, 1066 (1982), [Erratum: *Phys. Rev. Lett.* **56**, 2334 (1986)].
- [5] P. Koch, B. Muller, and J. Rafelski, *Phys. Rept.* **142**, 167 (1986).
- [6] C. M. Ko, *EPJ Web Conf.* **171**, 03002 (2018).
- [7] P. Danielewicz, R. Lacey, and W. G. Lynch, *Science* **298**, 1592 (2002).
- [8] T. Galatyuk, *JPS Conf. Proc.* **32**, 010079 (2020).
- [9] J. Aichelin and C. M. Ko, *Phys. Rev. Lett.* **55**, 2661 (1985).
- [10] J. Adamczewski-Musch *et al.*, *Phys. Lett. B* **793**, 457 (2019).
- [11] W. Cassing, E. Bratkovskaya, and A. Sibirtsev, *Nucl. Phys. A* **691**, 753 (2001).
- [12] A. Andronic, P. Braun-Munzinger, K. Redlich, and J. Stachel, *Nature* **561**, 321 (2018).
- [13] J. Cleymans and H. Satz, *Z. Phys. C* **57**, 135 (1993).
- [14] F. Becattini, M. Gazdzicki, and J. Sollfrank, *Eur. Phys. J. C* **5**, 143 (1998).
- [15] W. Florkowski, W. Broniowski, and M. Michalec, *Acta Phys. Polon. B* **33**, 761 (2002).
- [16] J. Cleymans, A. Förster, H. Oeschler, K. Redlich, and F. Uhlig, *Phys. Lett. B* **603**, 146 (2004).
- [17] K. Redlich and A. Tounsi, *Eur. Phys. J. C* **24**, 589 (2002).
- [18] G. Zeeb, M. Reiter, and M. Bleicher, *Phys. Lett. B* **586**, 297 (2004).
- [19] C. Fuchs, *Prog. Part. Nucl. Phys.* **56**, 1 (2006).
- [20] L. McLerran and R. D. Pisarski, *Nucl. Phys. A* **796**, 83 (2007).
- [21] K. Fukushima, T. Kojo, and W. Weise, *Phys. Rev. D* **102**, 096017 (2020).
- [22] B. B. Back *et al.* (E917 Collaboration), *Phys. Rev. C* **69**, 054901 (2004).
- [23] C. Alt *et al.* (NA49 Collaboration), *Phys. Rev. C* **78**, 044907 (2008).
- [24] J. Adam *et al.* (STAR Collaboration), *Phys. Rev. C* **102**, 034909 (2020).
- [25] P. Gasik *et al.*, *Eur. Phys. J. A* **52**, 177 (2016).
- [26] K. Piasecki *et al.* (FOPI Collaboration), *Phys. Rev. C* **91**, 054904 (2015).
- [27] G. Agakishiev *et al.* (HADES Collaboration), *Phys. Rev. C* **80**, 025209 (2009).
- [28] J. Adamczewski-Musch *et al.* (HADES Collaboration), *Phys. Lett. B* **778**, 403 (2018).
- [29] K. C. Meehan, *J. Phys. Conf. Ser.* **742**, 012022 (2016).
- [30] M. Anderson *et al.*, *Nucl. Instrum. Meth. A* **499**, 659 (2003).
- [31] W. J. Llope (for STAR), *Nucl. Instrum. Meth. A* **661**, S110 (2012).
- [32] C. A. Whitten (STAR), *AIP Conf. Proc.* **980**, 390 (2008).
- [33] M. Tanabashi *et al.* (Particle Data Group), *Phys. Rev. D* **98**, 030001 (2018).

- [34] I. Kisel (CBM), *J. Phys. Conf. Ser.* **1070**, 012015 (2018).
- [35] J. Adam *et al.* (STAR Collaboration), *Phys. Rev. Lett.* **126**, 162301 (2021).
- [36] Y. Xu *et al.*, *Nucl. Instrum. Meth.* **A614**, 28 (2010).
- [37] M. Shao *et al.*, *Nucl. Instrum. Meth.* **A558**, 419 (2006).
- [38] B. I. Abelev *et al.* (STAR Collaboration), *Phys. Rev. C* **79**, 034909 (2009).
- [39] G. Agakishiev *et al.* (HADES Collaboration), *Phys. Rev. Lett.* **103**, 132301 (2009).
- [40] S. Wheaton, J. Cleymans, and M. Hauer, *Comput. Phys. Commun.* **180**, 84 (2009).
- [41] M. Bleicher *et al.*, *J. Phys. G* **25**, 1859 (1999).
- [42] S. Bass *et al.*, *Prog. Part. Nucl. Phys.* **41**, 255 (1998).
- [43] J. Steinheimer and M. Bleicher, *J. Phys. G: Nucl. Part. Phys.* **43**, 015104 (2015).
- [44] V. Steinberg *et al.*, *Phys. Rev. C* **99**, 064908 (2019).
- [45] C. Alt *et al.* (NA49 Collaboration), *Phys. Rev. C* **77**, 024903 (2008).
- [46] S. V. Afanasiev *et al.* (NA49 Collaboration), *Phys. Rev. C* **66**, 054902 (2002).
- [47] B. Abelev *et al.* (ALICE Collaboration), *Phys. Rev. C* **91**, 024609 (2015).
- [48] B. I. Abelev *et al.* (STAR Collaboration), *Phys. Rev. C* **79**, 064903 (2009).
- [49] Y. Maeda *et al.*, *Phys. Rev. C* **77**, 015204 (2008).
- [50] P. Braun-Munzinger, K. Redlich, and J. Stachel, *Quark–Gluon Plasma 3*, 491–599 (2004).
- [51] C. Hartnack, H. Oeschler, Y. Leifels, E. L. Bratkovskaya, and J. Aichelin, *Phys. Rept.* **510**, 119 (2012).
- [52] T. Song, L. Tolos, J. Wirth, J. Aichelin, and E. Bratkovskaya, *Phys. Rev. C* **103**, 044901 (2021).
- [53] G.-C. Yong, Z.-G. Xiao, Y. Gao, and Z.-W. Lin, (2021), arXiv:2105.10284 [nucl-th].